Available online at www.CivileJournal.org

Civil Engineering Journal

(E-ISSN: 2476-3055; ISSN: 2676-6957)

Vol. 12, No. 04, April, 2026

Dynamic Responses of a Cylindrical Lattice Shell Structure with Explosion Venting Holes Under Internal Explosion

Shiqi Fu [1, 2*], Xuanneng Gao [3]

[1] College of Engineering, Fujian Jiangxia University, Fuzhou 350100, China.

[2] Institute of Infrastructural Protection in Fujian Jiangxia University, Fuzhou 350100, China.

[3] College of Civil Engineering, Huaqiao University, Xiamen 361021, China.

Received 18 January 2026; Revised 15 March 2026; Accepted 21 March 2026; Published 01 April 2026

Abstract

This study investigates the dynamic response of cylindrical steel lattice shell structures subjected to internal explosions and evaluates the effectiveness of explosion venting holes in mitigating structural damage. A detailed numerical model was developed using ANSYS/LS-DYNA and validated against experimental results. The comparison shows good agreement in both overpressure and structural strain responses, confirming the reliability of the model. Internal explosions produce complex shock wave reflections and convergence within confined spaces, leading to severe structural responses that differ significantly from those caused by external explosions. Based on the validated model, a systematic parametric analysis was conducted to examine the effects of venting hole arrangement, venting ratio, charge mass, connection stiffness, and rise-to-span ratio. The results show that dome-mounted and evenly distributed venting holes with a venting ratio of approximately 50% provide the most effective mitigation performance. Compared with a fully confined configuration, this design reduces the peak internal energy by more than 85% and limits the maximum displacement to less than one-third of the baseline value. The results also indicate that a larger charge mass and higher connection stiffness increase the structural energy and deformation, while a larger rise-to-span ratio generally reduces the internal explosion response. The study highlights the importance of combining explosion venting design with geometric optimization to improve the blast resistance of cylindrical lattice shell structures. The findings provide useful guidance for the protective design of large-span structures exposed to internal explosion hazards.

Keywords: Internal Explosion; Cylindrical Lattice Shell Structure; Explosion Venting; Dynamic Response.

1. Introduction

It is well known that large-span steel spatial structures are widely used in landmark buildings such as airports and stadiums. If such structures are subjected to terrorist bomb attacks, the result can be severe property damage and significant social impact. Therefore, research on the blast protection and blast resistance of large-span steel spatial structures deserves serious attention from researchers [1, 2].

Studies show that the response of large-span steel spatial structures to internal explosions is very different from their response to conventional external explosions [3]. First, the shock wave under internal explosion undergoes multiple reflections and convergence. These effects significantly amplify the overpressure. As a result, the internal blast load

* Corresponding author: shiqi1007@fjjxu.edu.cn

https://doi.org/10.28991/CEJ-2026-012-04-022

acting on the structure is no longer determined solely by the scaled distance. Second, under internal explosion, the structural responses depend not only on traditional factors such as the explosive charge and the structural geometry. It is also strongly influenced by the enclosure system.

To further explore blast protection methods for large-span steel spatial structures under internal explosion, previous studies proposed an empirical formula for the peak overpressure of shock waves on spherical latticed shells [4, 5]. Also, the other research studies worked on the distribution of overpressure under internal explosion in cylindrical reticulated shell structures. An equivalent calculation method for internal blast loads was proposed [6, 7]. Regarding structural response and failure mechanisms, Gao & Fu investigated the response of spherical reticulated shells under different space high ratios. The results showed that adjusting the space high ratios and introducing proper venting holes can significantly reduce the internal explosion response of the structure [8]. Wang [9] and Ma [10] studied the failure mechanisms of spherical reticulated shells under internal explosion through experiments and numerical simulations. Li [11] and Fu [12] investigated the failure mechanisms of cylindrical reticulated shell structures under internal explosion by experiments and numerical simulations. Their results indicated that the connection stiffness between the main structure and the building enclosure plays a key role in determining the level of structural damage under internal explosion [11, 12]. In addition, to verify that scaled model tests of large-span steel spatial structures under internal explosion can reflect the behavior of the original structures, Fu and Wang studied similarity laws for cylindrical and spherical reticulated shells under internal explosion. Based on similarity laws, internal explosion model tests were conducted to validate the related research findings [13-16].

Blast protection research focuses not only on blast loads, structural responses, and failure mechanisms. Researchers have also paid considerable attention to explosion venting design [17-19]. Explosion venting design refers to installing venting components in the enclosure system. When an explosion occurs, these components open venting paths to release the internal explosion pressure. This helps minimize damage to the main structure [20-23]. Explosion venting design has been successfully implemented in various buildings and facilities, with venting components such as steel plates, concrete walls, gypsum boards, and glass windows [23-27]. Research indicates that parameters such as the location, venting ratio, and opening scheme of venting holes significantly influence the effectiveness of venting and the structural response [28-31]. For example, Zhang et al. [24] used numerical simulations to investigate the impact of preformed holes in square steel plates on the explosion response, finding that appropriately positioned holes can effectively reduce localized stress concentrations, thereby delaying the failure process.

However, current research primarily focuses on the venting components themselves, often overlooking the impact of explosion venting holes on the dynamic response of the major structure [32]. In particular, studies on the arrangement of explosion venting holes in steel latticed shell structures and their coupled influence on the internal explosion response of the major structure remain limited. Although some studies have addressed the overall failure modes of structures under internal explosions [15], there has been insufficient systematic investigation into how the location, venting ratio, and opening scheme of venting holes specifically affect the internal explosion response of the major structure. To address this research gap, this paper focuses on a typical cylindrical steel latticed shell structure utilizing a detailed three-dimensional numerical model established in ANSYS/LS-DYNA. This study systematically examines the dynamic response characteristics of a structure under internal explosions and the influence of explosion venting hole design parameters. Specifically, this paper explores the following aspects:

First, a detailed finite element model of the structure was developed, selecting appropriate material constitutive relations, considering the impact of connection stiffness between the major structure and the building envelope, and validating the model's reliability through existing experimental data. Second, the structural response under different venting hole configurations was analyzed, focusing on the coupling mechanisms between the location, venting ratio, and opening scheme of venting holes, as well as their effects on pressure reduction and structural deformation. Third, the influence of key parameters such as explosive charge, structural connection stiffness, and rise-to-span ratio on the response was further investigated, revealing their interaction mechanisms with venting design.

2. Numerical Model of Structure Under Internal Explosion

2.1. Finite Element Model

A single-layer cylindrical lattice shell structure with a one-way inclined bar configuration was selected as an example, and ANSYS/LS-DYNA was used to establish a detailed numerical model of the structure under internal explosion [33, 34]. As shown in Figure 1, the numerical model consists of a cylindrical lattice shell structure, a rigid ground, explosives, and an air domain.

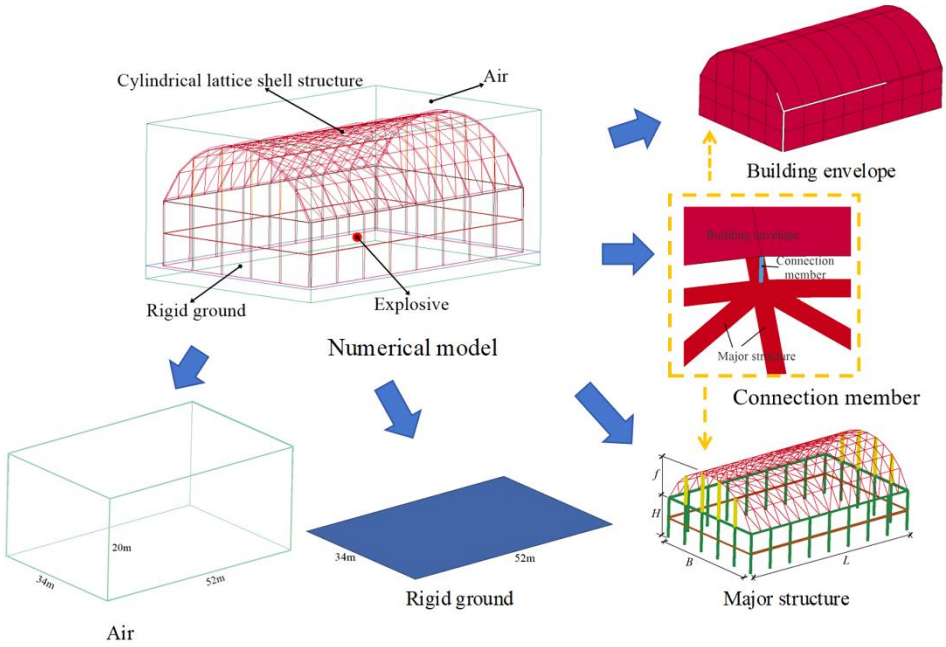

Figure 1. Numerical model of cylindrical lattice shell structure under internal explosion

The cylindrical lattice shell structure consists of the major structure and the building envelope. The parameters are shown in Table 1. The major structure has a length (*L*) of 48 m, a width (*B*) of 30 m, a height (*H*) of 8 m, and a rise (*f*) of 8 m. The primary members are modeled using Beam161 elements, while the building envelope is modeled using Shell163 elements [34]. The major structure and the building envelope are connected by 0.3 m connection components. All members of the structure are connected at common nodes, and the base of the columns is rigidly connected to the ground.

Table 1. Parameters of numerical model

Description	Value	Element type / Modeling method
Major structure	*L*=48 m, *B*=30 m, *H*=8 m, *f*=8 m	Beam161
Building envelope	*t*=0.003 m	Shell163
Connection members	*l*=0.3 m, *d*=0.03, EA/*l*= E*d*2*π*/4*l*= 4.45×105 N/m	Beam161
Rigid ground	52 m×34 m	Shell163
Air	52m ×34m ×20m	Solid164
Explosive	150 kg	Volume fraction

The air domain surrounds the structure and rigid ground, with overall dimensions of 50 m×50 m×16 m, and is modeled using Solid164 elements [34]. To balance computational accuracy and efficiency, the mesh size of the air domain is set to 0.5 m. The boundary of the air domain is defined as a transmission boundary to simulate the explosion in an infinite space [34]. The explosive charge is modeled using the volume fraction method and is located at the center of the structure, 1.2 m above the ground [34]. The ALE (arbitrary Lagrangian–Eulerian) method is used to compute the numerical model of the cylindrical lattice shell structure under internal explosion loads, accounting for the fluid-structure interaction between the shock wave and the structure [34].

2.2. Material Model

The materials for the major structure, building envelope, and connection components were made of Q235 steel. To account for the strain rate effect and strain hardening behavior of the steel under high-speed impact loading, the Johnson-Cook constitutive model was employed to simulate the dynamic mechanical response of the steel. The specific formulation of the model is provided in Equation 1 [34].

$$\sigma = (A_1 + A_2\varepsilon^n)(1 + A_3 \ln \dot{\varepsilon}^*)(1 - T^{*n_t}) \quad (1)$$

where σ, ε, $\dot{\varepsilon}^*$ and T^* represent the equivalent flow stress, the equivalent plastic strain, the relative strain rate and the relative temperature, respectively [34]. In this context, $\dot{\varepsilon}^* = \dot{\varepsilon}/\dot{\varepsilon}_0$, while $\dot{\varepsilon}$ and $\dot{\varepsilon}_0$ are the strain rate and the strain rate under quasi-static loading, respectively. $1 - \mathrm{T}^{*\mathrm{n_t}}$ represents the temperature softening effects [34]. Although detonation

produces extremely high temperatures near the explosive, the structural response is governed by the propagating blast wave rather than thermal effects. The high-temperature zone is confined to a small region around the charge. By the time the blast wave reaches the structure, the steel has not experienced a significant temperature rise. Therefore, for both the experiments and numerical simulations conducted at room temperature, temperature softening can be neglected. Accordingly, Equation 1 is simplified to Equation 2.

$$\sigma = (A_1 + A_2\varepsilon^n)(1 + A_3 \ln \dot{\varepsilon}^*) \tag{2}$$

where, A_1, A_2, A_3 and n are undetermined parameters that can be calibrated by experiment and are shown in Table 2 [12, 15].

Table 2. Johnson-Cook constitutive model parameters of the Q235 [12, 15]

A_1	A_2	n	A_3
320.7556×10^6	582.102×10^6	0.3823	0.0255

The air was simulated by MAT_NULL, and the state equation *EOS_LINEAR_POLYNOMIAL was adopted, as follows [34].

$$\begin{aligned} p_0 &= C_0 + C_1\eta + C_2\eta^2 + C_3\eta^3 + (C_4 + C_5\eta + C_6\eta^2)\cdot E_{air} \\ \eta &= 1/V_{air} - 1 \end{aligned} \tag{3}$$

where p_0 is the initial pressure of air. C_0, C_1, C_2, C_3, C_4, C_5 and C_6 are the material parameters of air. E_{air} and V_{air} represent the energy per unit volume and the relative volume of air, respectively. The values are shown in Table 3, where, and are the density, initial relative volume and initial internal energy of air, respectively.

Table 3. Material parameters of air [34]

ρ_{air}/kg·m^{-3}	C_0	C_1	C_2	C_3	C_4	C_5	C_6	$V_{0,air}$/J·m^{-3}	$E_{0,air}$
1.29	0	0	0	0	0.4	0.4	0	2.5×10^5	1.0

The explosive used was TNT, defined with *MAT_HIGH_EXPLOSIVE_BURN, and the equation of state was typically represented by the JWL model, as shown Equation 4:

$$P = A\left(1 - \frac{\omega}{R_1V}\right)e^{-R_1V} + B\left(1 - \frac{\omega}{R_2V}\right)e^{-R_2V} + \frac{\omega E_0}{V} \tag{4}$$

where, P is the pressure of shock waves. V is the relative volume. E_0 is the initial internal energy of the explosive. A, B, R_1, R_2, and ω are input parameters and are shown in Table 4, where ρ, D and P_{CJ} are the density of the explosive, the detonation velocity and the detonation pressure, respectively.

Table 4. Material parameters of explosive [8, 9,16]

ρ/kg·m^{-3}	D/m·s^{-1}	P_{CJ}/GPa	A/GPa	B/GPa	R_1	R_2	ω	E_0/J·m^{-3}	V_0
1630	6713	18.5	540.9	9.4	4.5	1.1	0.35	8.0×10^9	1.0

2.3. Validation of the Numerical Model

To investigate the reliability of the numerical modeling method, scaled model experiments of cylindrical lattice shell structures under internal explosion were conducted. The scaling coefficient of the experimental model was 0.1, and the charge masses were 50 g and 100 g, respectively. By comparing the experimental data with the simulation results, the accuracy of the modeling methods and material parameters used in the numerical simulations was validated.

Figure 2 illustrates the setup of the internal explosion experiments. As shown in Figure 2, the test apparatus consists of a 5 m×5 m×0.4 m concrete foundation platform and a cylindrical lattice shell structure. The cylindrical lattice shell structure is composed of the major structure and the building envelope. The upper lattice shell of the major structure is welded from seamless steel pipes and hollow ball joints, while the lower supporting structure is welded from square steel pipes and angle steel. The base of the major structure is bolted to the concrete foundation platform. The building envelope is made from hot-rolled steel plates with a thickness of 1.2 mm, completely enclosing the major structure. The major structure and the building envelope are connected by seamless steel pipes with a diameter of 30 mm. To minimize experimental errors, each explosive configuration was tested three times, and the average of these three tests was used as the final result.

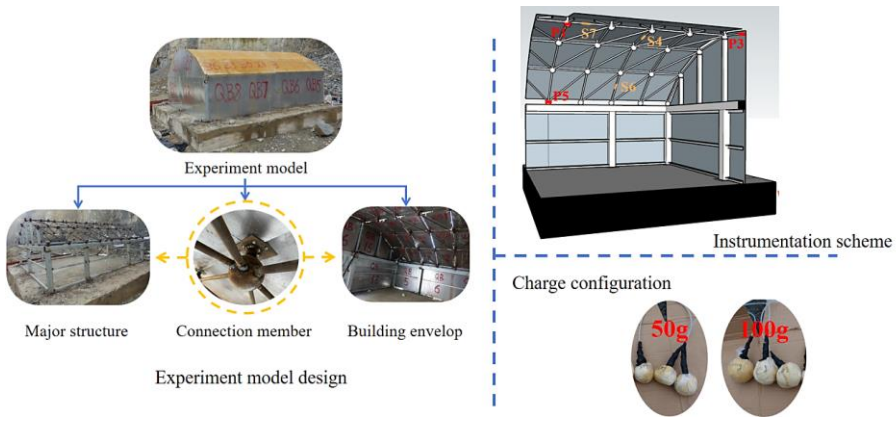

Figure 2. Experimental scheme for cylindrical lattice shell structure under internal explosion

Table 5 presents a comparison between the experimental results and simulation results, providing a detailed comparison of the overpressure under 100 g explosive conditions and the structural strain under 50 g explosive conditions. As shown in Table 5, under the 100 g explosive condition, slight differences are observed in the overpressure values at different measurement points. For instance, at point P1, the measured value is 0.06993 MPa, while the numerical simulation result is 0.06379 MPa, resulting in a relative error of 8.78%. The errors at points P3 and P5 are 5.25% and 13.65%, respectively. Overall, the simulation and experimental values exhibit good consistency in both magnitude and trend, demonstrating that the numerical model accurately captures the propagation of shock waves and overpressure distribution under internal explosions.

Table 5. Comparison between experimental results and simulation results

Overpressure under the 100g explosive charge condition				Structural strain under the 50g explosive charge condition			
Measuring points No.	**ΔP_{exp}/MPa**	**ΔP_{sim}/MPa**	**$\delta_{\Delta P}$/%**	**Measuring points No**	**ε_{exp}/MPa**	**ε_{sim}/MPa**	**δ_{ε}/%**
P1	0.06993	0.06379	8.78	S4	387.13	404.48	4.29
P3	0.05007	0.04744	5.25	S6	476.87	476.55	0.07
P5	0.07006	0.06050	13.65	S7	372.48	380.82	2.19

Notes: ΔP_{exp} and ΔP_{sim} represent the overpressure obtained from the experiment and numerical simulation, respectively. $\delta_{\Delta P} = |(\Delta P_{exp} - \Delta P_{sim})/\Delta P_{exp}| \times 100\%$.
ε_{exp} and ε_{sim} represent the structural strain obtained from the experiment and numerical simulation, respectively. $\delta_{\varepsilon} = |(\varepsilon_{exp} - \varepsilon_{sim})/\varepsilon_{exp}| \times 100\%$.

The strain responses under the 50 g explosive condition also demonstrate excellent fitting accuracy. Taking the S6 measurement point as an example, the measured strain is 476.87 με, while the simulation result is 476.55 με, yielding a minimal error of only 0.07%. The errors at the S4 and S7 measurement points are also within acceptable limits (4.29% and 2.19%, respectively). This indicates that by carefully considering modeling details such as material constitutive parameters, the developed finite element model can accurately predict the structural response to internal explosions.

It should be noted that the above experiments were conducted on a scaled model. The subsequent work in this study involves simulations of the original model with charge masses below 200 kg, which do not reach the critical failure state. To ensure that the conclusions obtained from the scaled experiments can be extended to the original model carried out systematic investigations on similarity laws for cylindrical latticed shell structures under internal explosion. The results showed that scaled models with a scaling coefficient not less than 0.1 can accurately reproduce the critical failure mode, critical TNT mass, propagation characteristics of the shock wave, overpressure distribution, load effects, and structural responses of the original model under internal explosion. Therefore, the research framework of this study is illustrated in Figure 3. By comparing the experimental and numerical results of the scaled model, the validity of the numerical modeling approach and the selection of material parameters can be verified. On this basis, combined with the similarity laws for cylindrical latticed shells under internal explosion, it is further demonstrated that the experimental and numerical results of the scaled model can effectively reflect the characteristics of the original model.

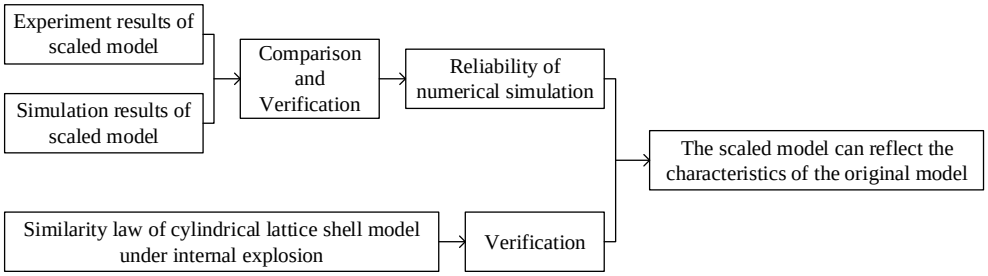

Figure 3. Flowchart of research methodology

3. Characteristics of Internal Explosion Response

3.1. Characteristics of Internal Blast Loading

A finite element model of the cylindrical lattice shell subjected to an internal explosion was established using the modeling approach and material parameters described in Section 2. The explosive charge was positioned at the geometric center of the structure, 1.5 m above the ground, with a charge mass of 150 kg. The overpressures of the shock waves at the dome region of the cylindrical reticulated shell (Location A) and at the corner region (Location B) were extracted to examine the propagation characteristics of shock waves under internal explosion.

The time-history curves of overpressure at locations A and B are presented in Figure 4. Immediately following detonation, the shock wave propagates outward and subsequently impinges upon the enclosure system, including both the wall and the roof. The internal blast loads are transferred to the main structure through the connectors between the enclosure components and the main structure. Thereafter, the shock waves are influenced by reflections from the ground and enclosure surfaces, gradually converging toward the structural corners and forming a shock-wave convergence phenomenon. As shown in Figure 4, a pronounced secondary reflection is observed in the dome region (Location A), whereas a noticeable convergence effect occurs in the corner region (Location B). Ultimately, the shock waves within the structure either mutually cancel or superimpose. Although the resulting patterns appear irregular, the peak overpressures remain relatively low. This indicates that, under internal explosion, the primary internal blast loading on the structure is dominated by the initial shock wave and that the effects of reflection and convergence of the shock waves should not be neglected

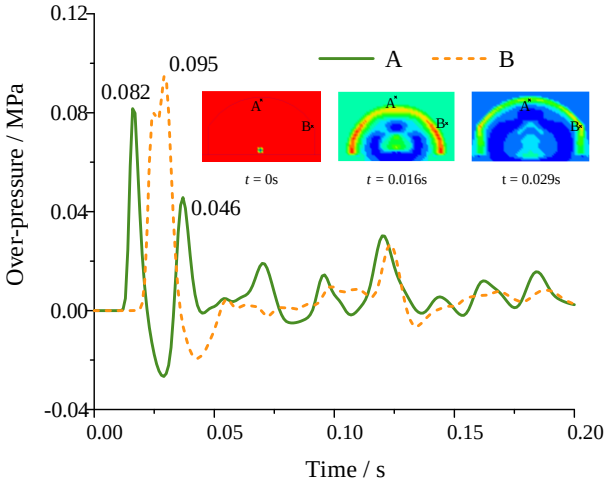

Figure 4. Propagation characteristics of shock waves under internal explosion

3.2. Internal Explosion Responses of Structures

To study the influence of internal blast loading on the structural response, two configurations were considered: a fully confined structure and a vented structure (Figure 5-a). A comparative analysis of their responses was conducted, and the corresponding results are shown in Figures 5-b and 5-c.

Figure 5-b illustrates the time-history curves of internal energy for the cylindrical lattice shell structure under internal explosion. During the initial stage, the internal energy of both configurations increases rapidly. The internal energy of the confined structure reaches a peak value of 843.3 kJ at approximately 0.15 s, whereas the vented structure attains only 617.05 kJ, corresponding to a reduction of approximately 26.8%. Following a brief oscillation, the internal energy in both configurations gradually stabilizes. Due to the release of a substantial portion of the blast energy through the vent holes, the vented structure exhibits a stable internal energy of approximately 480 kJ, which is approximately 25% lower than that of the confined structure. These results demonstrate that the vented configuration effectively mitigates the reflection and convergence effects of shock waves under internal explosion, thereby significantly reducing the internal energy of the main structure.

Figure 5-c presents the displacement time-history curves of the cylindrical lattice shell structure under internal explosion. Similar to the internal energy response, the confined structure reaches its maximum displacement of 84.886 mm at approximately 0.18 s, whereas the vented structure exhibits a peak displacement of only 24.386 mm, corresponding to approximately 28.7% of that of the confined structure. Subsequently, both configurations exhibit continuously decaying oscillations. However, their peak displacement ranges and final steady-state displacements differ significantly. For the confined structure, the displacement range is relatively large, with a difference of

109.071 mm between the maximum and minimum displacements, and the displacement stabilizes at approximately 15 mm after oscillation. This indicates that the confined structure undergoes violent oscillations under the internal explosion and experiences irreversible residual deformation. In contrast, the vented structure shows a displacement difference of 72.466 mm between its maximum and minimum values, which is approximately 66.44% of that of the confined structure. Moreover, the oscillation amplitude of the vented structure is relatively small, and it exhibits essentially no residual deformation. This suggests that the main structure of the vented configuration remains largely undamaged. This behavior is attributed to the release of a large portion of the internal explosive energy through the venting holes, so that the main structure no longer bears the full internal explosive load, thereby significantly reducing its deformation.

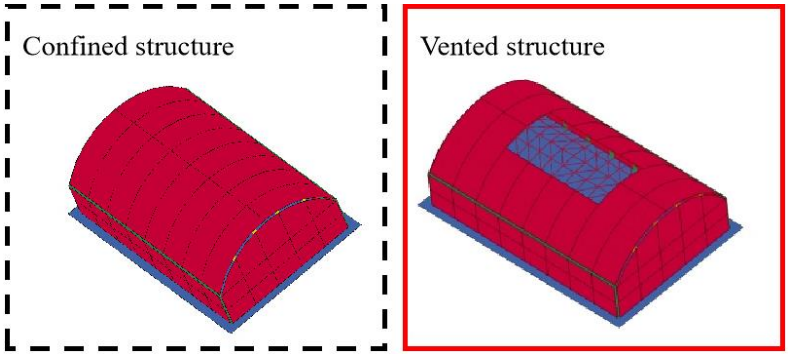

(a) Schematic diagram of the operating conditions

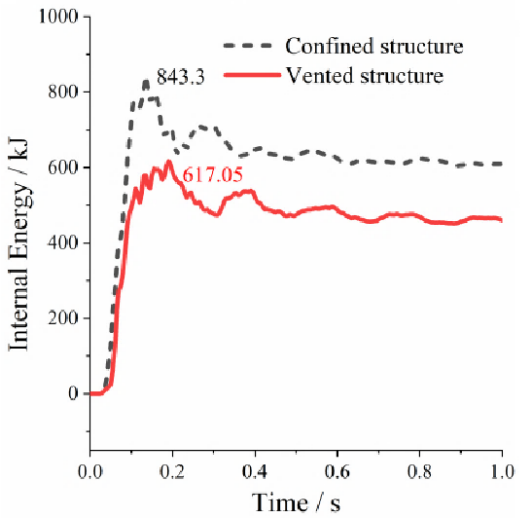

(b) Time-history curve of internal energy

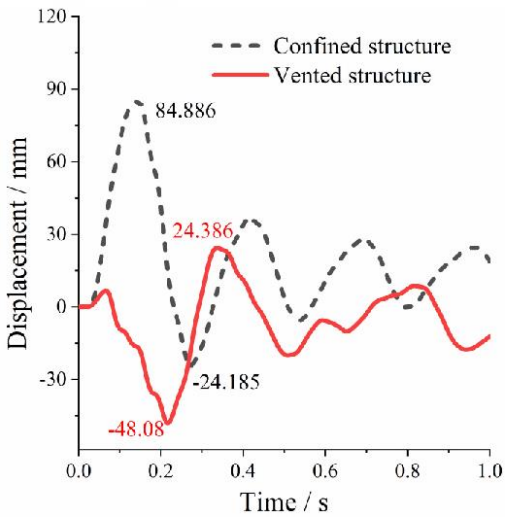

(c) Time-history curve of displacement

Figure 5. Internal explosion responses of cylindrical lattice shell structure

4. Influences of Explosion Venting Holes on Responses

As demonstrated by the above analysis, designing venting holes of appropriate size and placement on the building envelope can effectively suppress the accumulation of internal energy and mitigate the deformation response of the structure under internal explosion. Properly designed venting openings not only substantially reduce the peak internal energy and displacement values but also shorten the duration of structural oscillations, thereby enhancing the dynamic stability of the structure.

To determine the optimal venting configuration for a cylindrical lattice shell structure subjected to an internal explosion, a parametric study was conducted by varying the location, proportion, and opening scheme of the venting holes. The effects of different venting configurations on the structural responses were comparatively analyzed.

4.1. Location of Explosion Venting Holes

Figure 6-a illustrates three venting configurations with different hole locations: a structure without venting holes ("No holes"), a structure with holes on the dome ("Dome-mounted holes"), and a structure with holes on the wall ("Wall-mounted holes"). Except for the hole location, all other parameters—such as the venting ratio and opening scheme—are kept consistent.

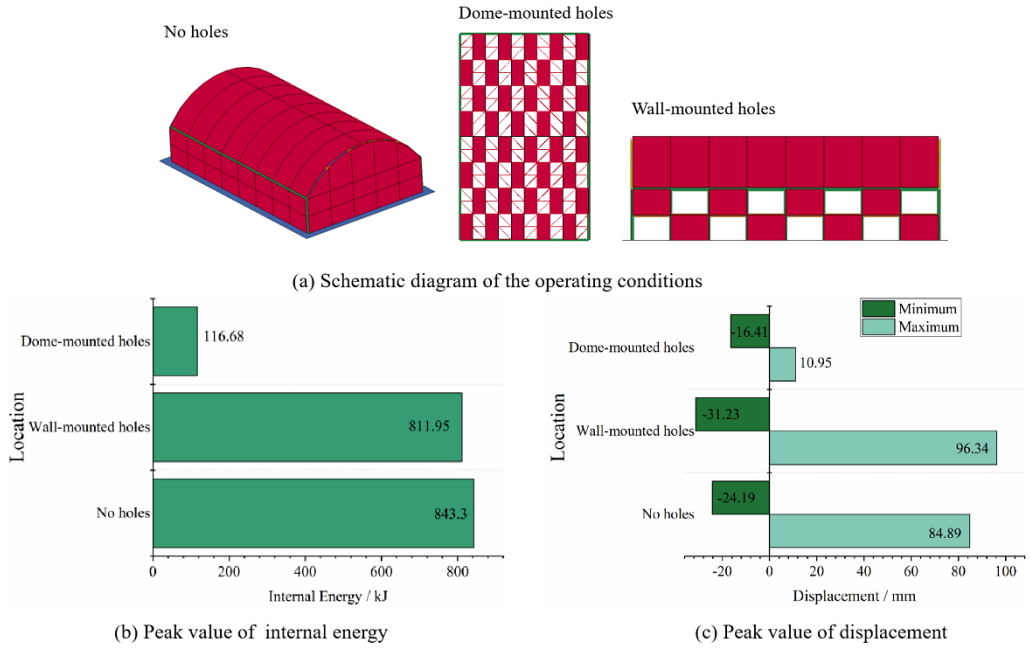

Figure 6. Comparison of internal explosion responses under different venting hole locations

As shown in Figures 6-b and 6-c, the peak internal energy and displacement of the cylindrical lattice shell structure under three working conditions are compared. The internal energy of the main structure is significantly affected by the location of the venting holes. The structure without holes exhibits the highest peak internal energy of 843.3 kJ, indicating severe energy accumulation under fully confined conditions. In contrast, the structure with wall-mounted holes reduces the peak internal energy to 811.95 kJ, corresponding to a 3.72% reduction, indicating only a modest mitigation effect. However, the effectiveness of wall-mounted venting remains limited. The structure with dome-mounted holes shows the lowest peak internal energy at only 116.68 kJ, representing an 86.16% reduction compared to the structure without holes, highlighting that dome-mounted holes are substantially more effective in mitigating internal energy under internal explosion.

Further analysis of the peak displacement responses reveals that variations in venting hole location lead to different levels of structural deformation. The structure with wall-mounted holes exhibits the largest displacement response, with a maximum displacement of 96.34 mm and a minimum displacement of -31.23 mm. This may be attributed to a reduction in the overall lateral stiffness caused by the introduction of wall-mounted holes, which weakens the lateral restraint and increases the susceptibility of the lower supporting columns to buckling under internal explosion. The structure without holes shows a slightly smaller displacement range, with a maximum of 84.89 mm and a minimum of -24.19 mm. In contrast, the structure with dome-mounted holes demonstrates a markedly smaller displacement response, with a maximum of only 10.95 mm, indicating that dome-mounted holes can effectively release explosion energy without substantially compromising structural stability.

By combining the internal energy and displacement results, it is evident that dome-mounted holes provide a more favorable balance between energy mitigation and structural safety. On the one hand, they significantly reduce the internal energy transmitted to the main structure; on the other hand, they maintain structural stability and effectively limit dynamic displacements, demonstrating strong practical applicability. In contrast, although wall-mounted holes offer limited mitigation of internal energy, they noticeably reduce structural stiffness and increase the risk of excessive deformation. Therefore, for the blast-resistant design of cylindrical lattice shell structures subjected to internal explosion, priority should be given to dome-mounted holes to achieve effective energy relief without compromising structural integrity.

4.2. Proportion of Explosion Venting Holes

To examine the influence of the venting ratio on the internal explosion response of the cylindrical lattice shell structure, three configurations were analyzed, as illustrated in Figure 7-a: one without venting holes (0%) and two with venting ratios of 20% and 50%. Except for the venting ratio, all other parameters—including location and opening scheme—were kept constant.

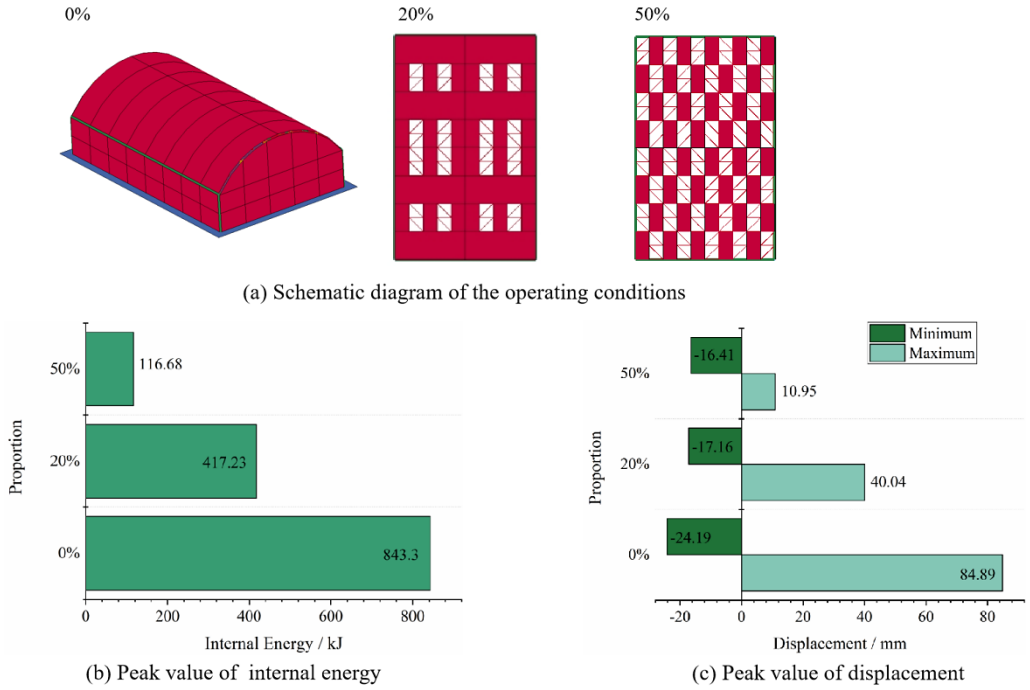

Figure 7. Comparison of internal explosion responses under different venting ratios

The peak internal energy and peak displacement of the structure under the three venting ratios are presented in Figures 7-b and 7-c. As shown in Figure 7-b, the venting ratio exerts a pronounced influence on the internal energy transmitted to the main structure under internal explosion. Increasing the venting ratio from 0% to 50% leads to a substantial reduction in internal energy, with peak values of 843.3 kJ (0%), 417.23 kJ (20%), and 116.68 kJ (50%), respectively. This trend demonstrates that a larger venting area effectively weakens the reflection and convergence of shock waves, thereby mitigating the internal energy accumulation in the main structure. Notably, at a venting ratio of 50%, the peak internal energy decreases to only 13.8% of that of the fully confined structure, highlighting the superior mitigation capacity of larger venting ratios.

Figure 7-c further illustrates the displacement responses under different venting ratios. A higher venting ratio results in significantly reduced displacement amplitudes. The fully confined structure exhibits a severe peak displacement range of 109.08 mm, which decreases to 57.20 mm and 27.36 mm for the 20% and 50% venting configurations, respectively. This suggests that increasing the venting area not only reduces internal energy but also indirectly mitigates structural deformation by weakening the reflection and convergence of shock waves, thereby enhancing overall structural stability.

Overall, increasing the venting ratio is effective in reducing the internal energy of the main structure and alleviating deformation induced by internal explosions. Although a 20% venting ratio reduces internal energy by approximately 50%, its mitigation effect on structural deformation is significantly less pronounced compared to the 50% configuration. Therefore, if internal energy reduction is prioritized as the primary design criterion for blast resistance, increasing the venting ratio to 50% is preferable. Conversely, if structural stability serves as the critical constraint, the venting ratio should be carefully optimized within the range of 20% to 50% to balance engineering practicality and structural performance.

4.3. Opening Scheme of Explosion Venting Holes

Figure 8-a presents three venting configurations with different opening schemes: a fully confined structure (“No holes”), a structure with clustered holes (“Clustered holes”), and a structure with uniformly scattered holes (“Scattered holes”). Except for the opening scheme, all other parameters—including hole location and venting ratio—are kept constant.

Figures 8-b and 8-c illustrate the coupled influence of the opening scheme on the internal energy and structural deformation. As shown in Figure 8-b, the scattered-hole configuration achieves the most substantial reduction in internal energy, with a peak value of only 116.68 kJ, corresponding to 13.8% of that of the fully confined structure and 15.4% of that of the clustered-hole configuration. This demonstrates that uniformly distributed venting holes can establish more efficient pressure-relief pathways, thereby weakening the reflection and convergence of shock waves and significantly reducing the internal energy transmitted to the main structure.

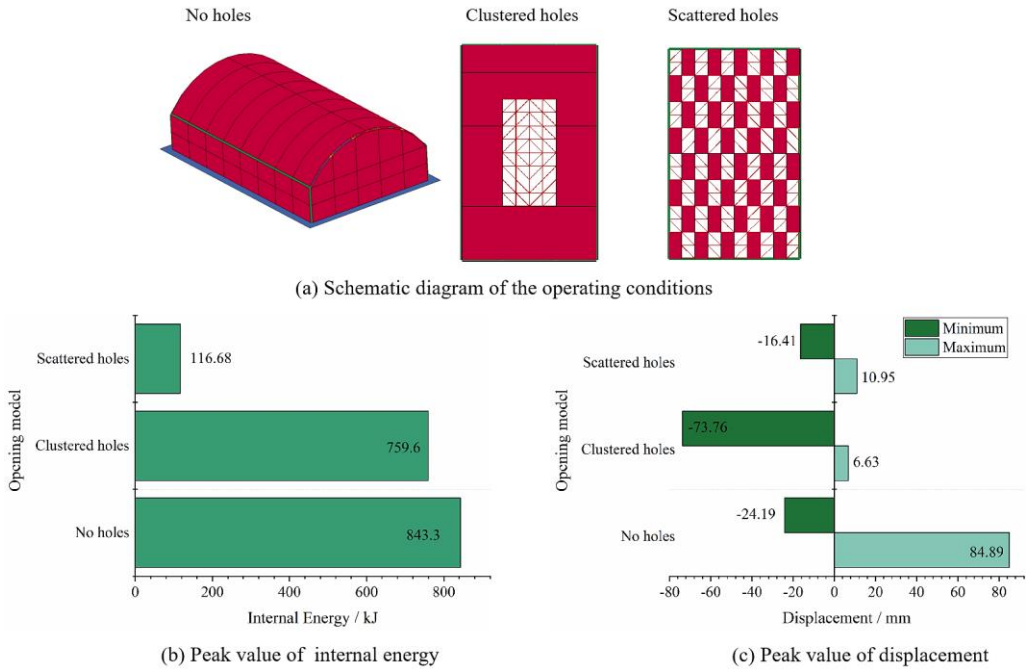

(a) Schematic diagram of the operating conditions

(b) Peak value of internal energy

(c) Peak value of displacement

Figure 8. Comparison of internal explosion responses under different opening schemes

In contrast, although the clustered-hole configuration provides limited energy release, the internal energy in the main structure remains as high as 759.6 kJ, only slightly lower than that of the fully confined configuration. This indicates that concentrating the venting openings within a localized region is insufficient to form a stable and effective venting mechanism, thereby limiting its ability to mitigate internal explosion energy.

As shown in Figure 8-c, the peak displacement ranges of the scattered-hole and clustered-hole configurations are 27.36 mm and 80.39 mm, respectively, representing decreases of 74.92% and 26.3% relative to the fully confined structure. Notably, the clustered-hole configuration exhibits a minimum displacement of −73.76 mm, which is far greater in magnitude than that of the fully confined (-24.19 mm) and scattered-hole (-16.41 mm) configurations. In addition, the clustered-hole configuration may also exhibit residual negative deformation after the explosion, indicating that the main structure experiences damage and faces an increased risk of instability. This behavior may result from the fact that the clustered-hole configuration primarily vents the initial shock wave while providing limited capability to reduce subsequent wave reflections and focusing effects.

Although clustered holes are advantageous in terms of design simplicity and ease of implementation, they may induce structural damage and increase the likelihood of localized failure in vulnerable regions. By combining the analyses of internal energy and displacement responses, the scattered-hole configuration demonstrates superior performance in both mitigating internal energy and maintaining structural stability. Its effective venting capability substantially weakens shock wave reflection and convergence effects under internal explosion and significantly suppresses structural deformation in both outward and inward directions.

5. Discussion of Different Factors

Based on the analysis presented in Section 4, the optimal arrangement of explosion venting holes for cylindrical lattice shell structures subjected to internal explosions is to place them on the dome enclosure. The venting ratio should be maximized within practical engineering constraints, and the venting holes should be uniformly distributed across the surface. As shown in Figure 9, such a configuration provides a more rational and effective approach for mitigating the effects of internal explosions.

However, the dynamic response of the structure under internal explosion is influenced by several critical factors, including the explosive charge mass, the stiffness of the connections between the main structure and the building envelope, and the rise-to-span ratio. To further optimize the venting design for cylindrical lattice shell structures, a series of parametric case studies is conducted based on the configuration illustrated in Figure 9, as summarized in Table 6. These cases aim to investigate the influences of the explosive charge mass, structural connection stiffness, and rise-to-span ratio on the structural response under internal explosion loading.

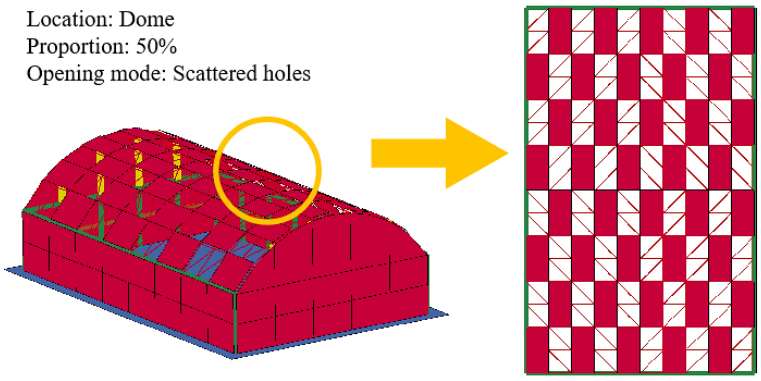

Figure 9. An effective explosion venting strategy

Table 6. Parameters influencing the internal explosion response of cylindrical lattice shell structures

Parameters	Value
Charge mass / kg	50, 100, 150, 200
Connection stiffness / $N \cdot m^{-1}$	2.2×10^8, 3.4×10^8, 5.0×10^8, 6.7×10^8, 8.8×10^8
Rise-to-span ratio	6/30, 8/30, 10/30, 12/30

5.1. Effect of Charge Mass

Figure 10 compares the peak internal energy responses of a fully confined structure and a vented structure under varying explosive charge masses. As shown in Figure 10, the internal energy of the confined structure shows a marked upward trend as the charge mass increases. Specifically, the internal energy rises sharply from 190.94 kJ at 50 kg to 968.71 kJ at 200 kg—an increase exceeding 400%.

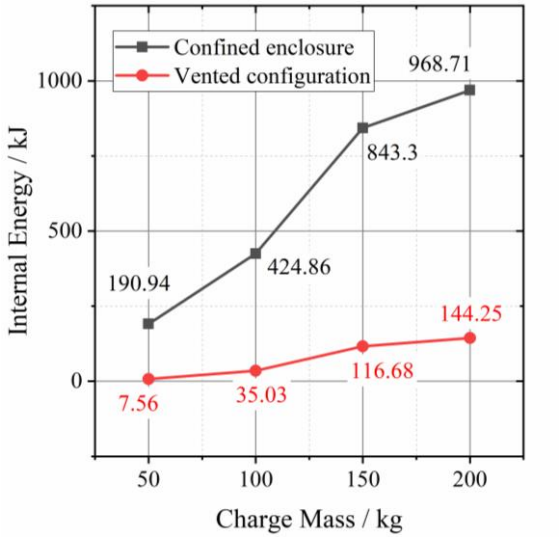

Figure 10. Influence of charge mass on the internal energy of structure under internal explosion

In contrast, the vented structure shows a much slower growth, with internal energy increasing only from 7.56 kJ to 144.25 kJ. This pronounced difference highlights the effectiveness of explosion venting in suppressing internal energy buildup. The superior performance of the vented structure is primarily attributed to the presence of dedicated pressure relief pathways, which significantly reduce shock wave reflection and convergence within the structure, thereby mitigating energy accumulation in the major structure.

Further analysis of the growth trends indicates that the confined structure displays an approximately linear increase in internal energy, whereas the vented structure exhibits a decelerated rise beyond a charge mass of 100 kg. This behavior suggests that venting becomes increasingly effective under high-mass explosive loading. The associated mechanism of reducing internal energy plays a critical role in structural safety design, particularly in scenarios involving large explosive charges.

Figure 11 presents the peak displacement responses of the structure under varying explosive charge masses, further validating the influence of explosion venting holes on the performance of the major structure under internal explosion. In the confined structure, the maximum displacement increases from 39.37 mm to 94.09 mm, while the minimum displacement decreases from -16.83 mm to -28.38 mm, both exhibiting a consistent upward trend in magnitude. This indicates that structural responses intensify markedly with increasing charge mass. In contrast, although the vented structure also shows a rise in displacement peaks with increasing explosive loads, the rate of increase is substantially lower. The maximum displacement increases modestly from 4.39 mm to 13.03 mm, and the minimum displacement increases from -5.64 mm to -18.59 mm. Notably, while the minimum displacement in the vented structure does increase, its overall magnitude remains relatively moderate, suggesting that residual negative deformation is avoided and that the structural system retains a high degree of stability.

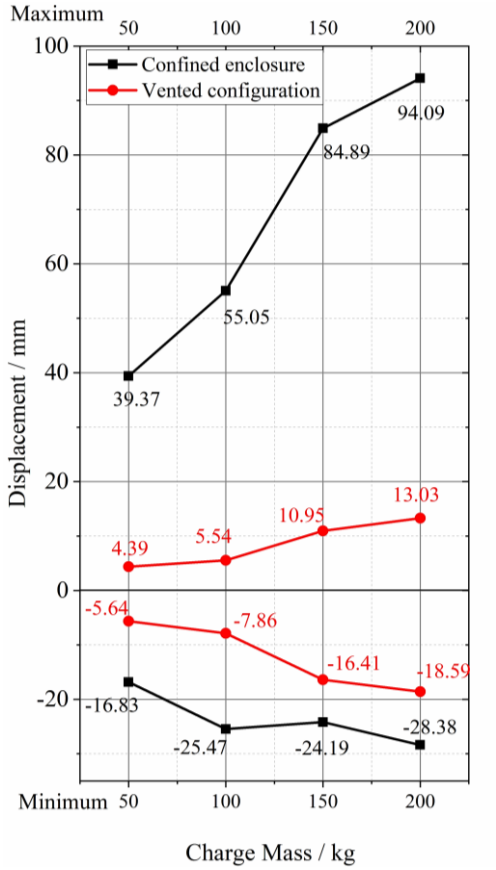

Figure 11. Influence of charge mass on the displacement of structure under internal explosion

As evidenced by the combined results in Figures 10 and 11, under higher charge masses, the internal blast load field within the confined structure becomes extremely intense, resulting in a pronounced amplification of the structural responses. The incorporation of venting design effectively suppresses the reflection and convergence effects of shock waves under internal explosion, thereby significantly mitigating the severity of structural responses. Moreover, the mitigation effect becomes increasingly pronounced with increasing charge mass. These findings demonstrate that explosion venting represents an efficient and reliable approach for blast-resistant design.

5.2. Effect of Connection Stiffness

Studies have demonstrated that the connection stiffness between the major structure and the building envelope exerts a profound influence on the dynamic response of cylindrical lattice shells under internal explosion [15, 16]. Figure 12 compares the peak internal energy responses of the major structure under both confined and vented configurations. As shown in Figure 12, the peak internal energy of the confined structure exhibits a gradual upward trend with increasing connection stiffness, rising from 810.52 kJ at 2.2×10^8 N·m^{-1} to 896.1 kJ at 8.88×10^8 N·m^{-1}. The increase becomes particularly pronounced when the connection stiffness exceeds 5.0×10^8 N·m^{-1}. This suggests that higher connection stiffness leads to greater internal energy accumulation in the major structure, thereby increasing the risk of structural damage.

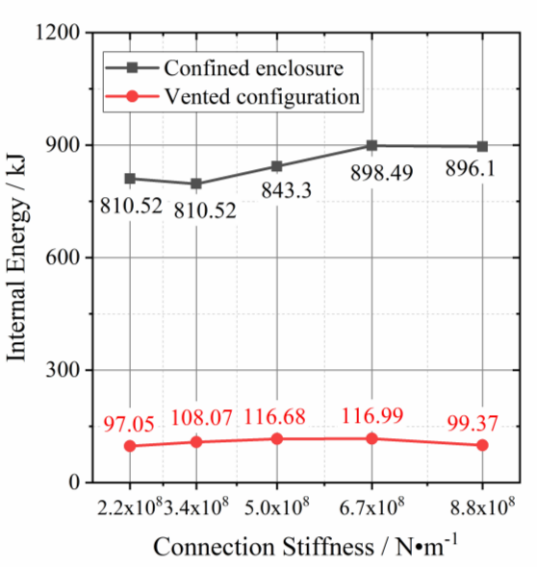

Figure 12. Influence of connection stiffness on the internal energy of structure under internal explosion

In contrast, the vented structure consistently maintains a low level of internal energy, varying within a narrow range of 97.05 kJ to 116.99 kJ, and exhibits minimal sensitivity to changes in connection stiffness. This behavior indicates that well-defined venting pathways effectively suppress the reflection and convergence of shock waves generated by internal explosions, thereby limiting the generation of internal explosive energy in the major structure and significantly reducing the influence of connection stiffness on its internal energy.

Figure 13 further illustrates the displacement responses of the structure under varying connection stiffnesses. For the confined structure, the displacement span remains consistently large over the entire stiffness range. At a connection stiffness of 2.2×10^8 N·m^{-1}, the span reaches 134.43 mm (from -46.19 mm to 88.24 mm). Although increasing the connection stiffness slightly reduces the minimum displacement and limits the maximum displacement at higher stiffness levels, the span remains as large as 109.05 mm at 8.8×10^8 N·m^{-1}. This indicates that, under a constant charge mass, increasing connection stiffness alone provides only limited control over the extreme deformation under internal explosion.

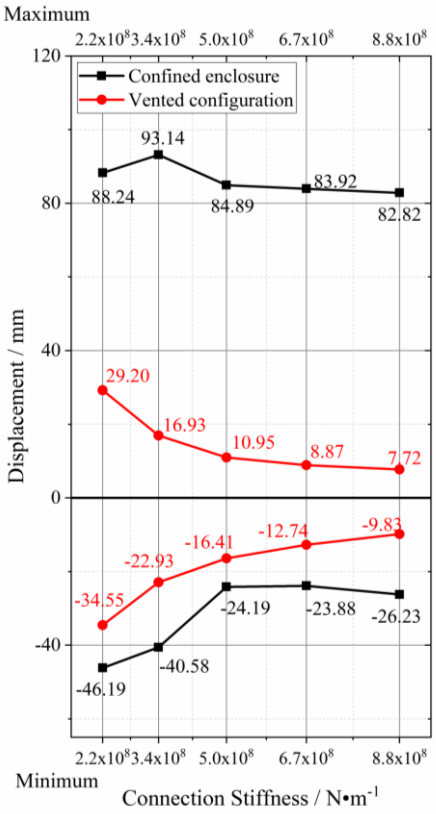

Figure 13. Influence of connection stiffness on the displacement of structure under internal explosion

In contrast, the vented structure exhibits a pronounced reduction in displacement span with increasing connection stiffness. Specifically, the displacement span decreases from 63.75 mm at 2.2×10^8 N·m^{-1} (29.20 mm to -34.55 mm) to only 17.55 mm at 8.8×10^8 N·m^{-1} (7.72 mm to -9.83 mm), corresponding to a reduction of approximately 72.5%. At all stiffness levels, the displacement span of the vented structure is less than 50% of that of the confined structure, demonstrating a substantial attenuation of the deformation amplitude.

This pronounced reduction in displacement span results from two main factors. Increased connection stiffness constrains global structural deformation. Meanwhile, the venting mechanism suppresses the reflection and convergence effects of shock waves under internal explosion and limits the generation of internal explosive energy. As a result, the vented configuration consistently exhibits much smaller displacement spans than the confined structure at all connection stiffness levels. This demonstrates its superior effectiveness in reducing blast-induced deformation and improving structural stability under internal explosion.

5.3. Effect of the Rise-to-span Ratio

The rise-to-span ratio is a fundamental geometric parameter of cylindrical lattice shell structures. Investigating the internal energy and displacement responses of both confined and vented configurations under varying rise-to-span ratios is crucial for improving the general applicability of explosion venting designs in practice.

Figure 14 presents the internal energy responses of confined and vented structures under different rise-to-span ratios. For the confined structure, the internal energy decreases markedly as the rise-to-span ratio increases. It drops from 1702 kJ at a ratio of 6/30 to 415.61 kJ at 12/30. This trend is mainly associated with the increase in internal geometric volume, which weakens the accumulation of explosion energy.

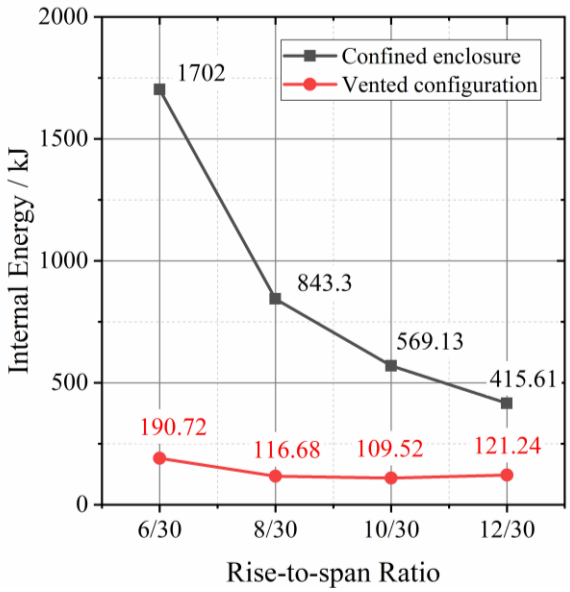

Figure 14. Influence of rise-to-span ratio on the internal energy of structure under internal explosion

In contrast, the vented structure maintains much lower internal energy levels owing to the presence of effective energy-release paths. With increasing rise-to-span ratio, the internal energy decreases only slightly, from 190.72 kJ to 121.24 kJ. This indicates that although the rise-to-span ratio contributes to internal energy reduction, its influence is secondary compared with that of venting, which plays a dominant role in reducing internal energy.

Figure 15 illustrates the displacement responses of confined and vented structures under different rise-to-span ratios. For the confined structure, the maximum displacement decreases sharply as the rise-to-span ratio increases, dropping from 191.12 mm at 6/30 to 27.59 mm at 12/30. Meanwhile, the minimum displacement increases from −34.85 mm to −18.50 mm. As a result, the displacement span is significantly reduced, indicating that a higher rise-to-span ratio effectively limits extreme deformation.

In contrast, the vented structure exhibits much smaller displacement spans over the entire range of rise-to-span ratios. The maximum displacement decreases moderately from 39.57 mm to 10.35 mm, while the minimum displacement increases from −19.51 mm to −11.87 mm. Consequently, the difference between the maximum and minimum displacements remains relatively small and changes only slightly with increasing rise-to-span ratio. This comparison highlights that although the rise-to-span ratio influences structural deformation, the vented configuration consistently maintains a much narrower displacement span than the confined structure, demonstrating superior deformation control under internal explosion.

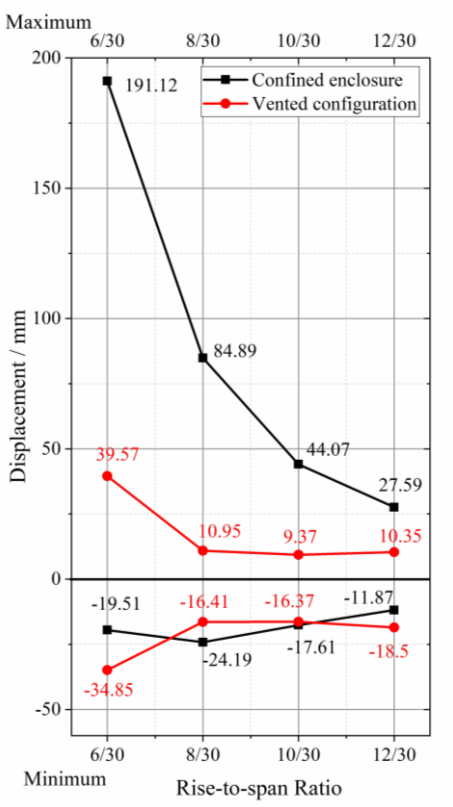

Figure 15. Influence of rise-to-span ratio on the displacement of structure under internal explosion

As seen from the above analysis, the rise-to-span ratio has a clear effect on the internal energy and displacement responses. Confined structures with smaller rise-to-span ratios show higher internal energy levels and larger deformation responses. As the rise-to-span ratio increases, the expansion of the internal volume promotes energy attenuation, leading to a pronounced reduction in structural displacement. In comparison, vented structures exhibit much smaller changes in internal energy due to the efficient release of explosion energy through venting openings, and displacement responses remain limited and stable. From a practical design perspective, increasing the rise-to-span ratio is an effective approach to mitigating internal explosion effects, whereas for structures with relatively small rise-to-span ratios, the implementation of explosion venting holes should be considered.

6. Conclusion

This study investigated the dynamic responses of cylindrical lattice shell structures subjected to internal explosions and evaluated the effectiveness of explosion venting holes in mitigating structural damage. A detailed numerical model was developed using ANSYS/LS-DYNA and validated with scaled experimental data, which showed good agreement in both overpressure and strain responses. The results confirm that internal explosions produce complex shock wave reflections and convergence within enclosed spaces, leading to severe structural responses. Introducing explosion venting holes provides effective pressure-relief paths that significantly weaken these shock wave interactions. Compared with fully confined structures, vented configurations reduce peak internal energy by more than 80% and peak displacement by over 70%, demonstrating the strong mitigation capability of explosion venting design.

The effectiveness of explosion venting is strongly influenced by the configuration of the openings. Parametric analyses show that vent location, venting ratio, and opening scheme all play important roles in controlling structural responses. Venting holes arranged on the dome are far more effective than those located on the sidewalls. Increasing the venting ratio substantially improves the pressure relief performance, and a ratio of approximately 50% provides the most efficient energy reduction. In addition, uniformly distributed openings perform better than clustered openings because they form more stable pressure-release pathways and reduce shock wave reflections more effectively. Further analyses indicate that the explosive charge mass, connection stiffness between the major structure and the building envelope, and rise-to-span ratio also influence internal explosion responses. Larger charge masses and higher connection stiffness tend to increase internal energy and deformation. In contrast, a larger rise-to-span ratio generally reduces the explosion response by increasing the internal volume. Overall, the results highlight that combining optimized venting design with appropriate structural geometry can significantly improve the blast resistance of cylindrical lattice shell structures and provide practical guidance for the protective design of large-span spatial structures exposed to internal explosion hazards.

7. Declarations

7.1. Author Contributions

Conceptualization, G.X.; methodology, F.S.; formal analysis, F.S.; investigation, F.S.; resources, F.S.; data curation, F.S. and G.X.; writing—original draft preparation, F.S.; writing—review and editing, F.S.; supervision, G.X.; funding acquisition, F.S. and G.X. All authors have read and agreed to the published version of the manuscript.

7.2. Data Availability Statement

The data presented in this study are available on request from the corresponding author.

7.3. Funding

This research was funded by the National Natural Science Foundation of China (Grant No. 51278208), the Science and Technology Project of Fujian Province (Grant No. 2022J01967), the National Fund Cultivation Project of Fujian Jiangxia University (Grant No. JXZ2024003), and the Institute of Infrastructural Protection in Fujian Jiangxia University.

7.4. Conflicts of Interest

The authors declare no conflict of interest.

8. References

[1] Hu, Y., Wu, C., Lukaszewicz, M., Dragos, J., Ren, J., & Haskett, M. (2011). Characteristics of confined blast loading in unvented structures. International Journal of Protective Structures, 2(1), 21–44. doi:10.1260/2041-4196.2.1.21.

[2] U.S. Department of Defense. (2008). Unified facilities criteria (UFC) 3-340-02: Structures to resist the effects of accidental explosions. U.S. Department of Defense, Washington, D.C., United States.

[3] Edri, I., Savir, Z., Feldgun, V. R., Karinski, Y. S., & Yankelevsky, D. Z. (2011). On blast pressure analysis due to a partially confined explosion: I. experimental studies. International Journal of Protective Structures, 2(1), 1–20. doi:10.1260/2041-4196.2.1.1.

[4] Wenbao, W., & Xuanneng, G. (2016). Overpressure peak formula of surface shock waves in single layer spherical lattice shell under the effect of internal explosion. Journal of Discrete Mathematical Sciences and Cryptography, 19(5–6), 1073–1090. doi:10.1080/09720529.2016.1253353.

[5] Duan, L. L., Gao, X. N., & Jiang, Y. (2014). Analysis for shock wave overpressure of spherical steel reticulated shell under internal explosion. Journal of Huaqiao University: Natural Science, 34(5), 557-562.

[6] Xie, W. W., Gao, X. N., & Jiang, Y. (2013). Calculation of shock wave overpressures of internal explosion within large-space steel reticulated dome. Guangxi Daxue Xuebao (Ziran Kexue Ban), 38(1), 16-22.

[7] Shiqi, F., & Xuanneng, G. (2025). Equivalent method for calculating internal blast loads in cylindrical lattice shell structure. Scientific Reports, 15(1), 27656. doi:10.1038/s41598-025-13066-4.

[8] Gao, X., & Fu, S. (2017). Influence of space height on the internal explosion response of single-layer spherical reticulated shell. Tumu Jianzhu Yu Huanjing Gongcheng/Journal of Civil, Architectural and Environmental Engineering, 39(4), 107–114. doi:10.11835/j.issn.1674-4764.2017.04.017.

[9] Wang, W. (2017). Study on the failure mechanism of spherical lattice shells under internal explosion. Master's thesis, Huaqiao University, Fujian, China.

[10] Ma, J. (2016). Blast loading and failure mechanism of single-layer reticulated domes subjected to interior blast. Master's thesis, Harbin Institute of Technology, Heilongjiang, China.

[11] Li, C. (2016). Failure mechanism and explosion prevention methods of cylindrical lattice shells under internal explosion. Master's thesis, Huaqiao University, Fujian, China.

[12] Fu, S. (2020). Study on internal explosion effects and explosion-proof measures for cylindrical lattice shell structures. Master's thesis, Huaqiao University, Fujian, China.

[13] Fu, S., Gao, X., & Chen, X. (2018). The similarity law and its verification of cylindrical lattice shell model under internal explosion. International Journal of Impact Engineering, 122, 38–49. doi:10.1016/j.ijimpeng.2018.08.010.

[14] Xuanneng, G., Shiqi, F., Qian, L., Daohe, C., Qi, Z., Xin, C., & Wenbao, W. (2022). Dynamic scaling laws of spatial grid structures under inner explosion considering material and geometric distortions. Mechanics of Advanced Materials and Structures, 29(26), 5163–5176. doi:10.1080/15376494.2021.1949652.

[15] Wang, W., Gao, X., & Le, L. (2017). Study of the Similarities in Scale Models of a Single-Layer Spherical Lattice Shell Structure under the Effect of Internal Explosion. Shock and Vibration, 2017(1), 1–13. doi:10.1155/2017/9181729.

[16] Zhao, C. F., Chen, J. Y., Wang, Y., & Lu, S. J. (2012). Damage mechanism and response of reinforced concrete containment structure under internal blast loading. Theoretical and Applied Fracture Mechanics, 61(1), 12–20. doi:10.1016/j.tafmec.2012.08.002.

[17] Chippett, S. (1984). Modeling of vented deflagrations. Combustion and Flame, 55(2), 127–140. doi:10.1016/0010-2180(84)90022-1.

[18] Bauwens, C. R., Chaffee, J., & Dorofeev, S. B. (2011). Vented explosion overpressures from combustion of hydrogen and hydrocarbon mixtures. International Journal of Hydrogen Energy, 36(3), 2329–2336. doi:10.1016/j.ijhydene.2010.04.005.

[19] NFPA 68. (2018). Standard on Explosion Protection by Deflagration Venting. National Fire Protection Association (NFPA), Massachusetts, United States.

[20] Hernandez, F., Carcamo, L., Hao, H., Zhang, X., Contreras, N., & Astroza, R. (2025). Analysis of fuel storage tanks under internal deflagrations with different venting technologies: an experimental and numerical study. Engineering Failure Analysis, 167, 108948. doi:10.1016/j.engfailanal.2024.108948.

[21] Song, Y., Jiang, Y., & Zhong, W. (2024). Numerical study on the influence of venting interlayer structure on the explosion venting effects. International Communications in Heat and Mass Transfer, 156, 107714. doi:10.1016/j.icheatmasstransfer.2024.107714.

[22] Rui, S., Wang, Q., Wang, C., & Zhang, A. (2024). Effects of ignition location and vent area on the external explosion in vented hydrogen explosions. Process Safety and Environmental Protection, 183, 602–616. doi:10.1016/j.psep.2023.10.070.

[23] Zhou, B., Zhi, X., Song, Y., Li, Z., Fan, F., & Zhang, R. (2025). Experimental and numerical study of light, fragile vent covers under vented gas explosions. Engineering Structures, 322. doi:10.1016/j.engstruct.2024.119180.

[24] Zhang, C., Tan, P. J., & Yuan, Y. (2022). Confined blast loading of steel plates with and without pre-formed holes. International Journal of Impact Engineering, 163. doi:10.1016/j.ijimpeng.2022.104183.

[25] Liu, W., Shi, Y., Hao, H., & Zhang, X. (2021). Numerical analysis of dynamic responses of laminated glass window subjected to gas explosions. Engineering Structures, 238. doi:10.1016/j.engstruct.2021.112243.

[26] Guo, X., Li, Y., McCrum, D. P., Hu, Y., & Bai, Z. (2025). A reinforced concrete shear wall building structure subjected to internal TNT explosions: TNT location parameter study and new simplified uniformly distributed overpressure calculation model. Engineering Structures, 341 doi:10.1016/j.engstruct.2025.120867.

[27] Guo, X., Li, Y., McCrum, D. P., Hu, Y., Bai, Z., Zhang, H., Li, Z., & Wang, X. (2024). A reinforced concrete shear wall building structure subjected to internal TNT explosions: Test results and numerical validation. International Journal of Impact Engineering, 190. doi:10.1016/j.ijimpeng.2024.104950.

[28] Li, Y., Wu, W., Zhu, H., Wu, Z., & Du, Z. (2017). The influence of different pre-formed holes on the dynamic response of square plates under air-blast loading. Engineering Failure Analysis, 78, 122–133. doi:10.1016/j.engfailanal.2017.03.002.

[29] Sun, S., Wang, M., Gao, K., Zhao, T., & Guo, Q. (2018). Effect of vent conditions on internal overpressure time-history during a vented explosion. Journal of Loss Prevention in the Process Industries, 54, 85–92. doi:10.1016/j.jlp.2018.03.002.

[30] Langdon, G. S., Kriek, S., & Nurick, G. N. (2020). Influence of venting on the response of scaled aircraft luggage containers subjected to internal blast loading. International Journal of Impact Engineering, 141, 103567. doi:10.1016/j.ijimpeng.2020.103567.

[31] Sun, S., Qiu, Y., Xing, H., & Wang, M. (2020). Effects of concentration and initial turbulence on the vented explosion characteristics of methane-air mixtures. Fuel, 267. doi:10.1016/j.fuel.2020.117103.

[32] Yu, R., Qiu, Y., Xing, H., Xu, G., Wang, M., Li, B., Xie, L., & Sun, S. (2024). Experimental investigation on the dynamic response of vent plate under methane-air mixtures explosion load. Engineering Structures, 318. doi:10.1016/j.engstruct.2024.118471.

[33] Li, Y., & Ma, S. (1992). Explosion Mechanics. National Defense Industry Press, Beijing, China.

[34] Hallquist, J.O. (2007). LS-DYNA keyword user's manual (Version 971). Livermore Software Technology Corporation, California, United States.